Surface Temperature Measurements on Superconducting Cavities in Superfluid Helium

M. Fouaidy, T. Junquera, A. Caruette

Institut de Physique Nucléaire. CNRS - IN2P3 (Univ. Paris Sud)
BP 1 . 91406 ORSAY France

ABSTRACT

Two thermometry systems have been developed at the GECS (Groupe d'Etudes des Cavités Supraconductrices) laboratory: a scanning thermometer system routinely used for the 1.5 GHz monocell cavity studies and a fixed thermometer array used to investigate spatial surface resistance distribution on various SC removable endplates of a cylindrical TE011 mode cavity. Thermometers used in these systems are thermally insulated from the surrounding HeII bath by an epoxy housing ("epoxy" thermometers).

Accurate calibration of the fixed thermometers was conducted by using different test cells and the experimental results were compared to model calculations performed with a finite element computational code. Measured thermometer efficiency and linearity are in good agreement with numerical results. Some typical temperature maps of different Nb samples obtained with the TE011 array (40 epoxy thermometers) are discussed.

On the basis of numerical modelling results, a new type of thermometer with an improved efficiency has been designed. The thermal insulation against Helium II has been drastically improved by placing the sensitive part of the thermometer in a small vacuum jacket ("vacuum" thermometers). Two main goals have been reached with the first prototypes: improved efficiency by a factor of 2.5 - 3, and a bath temperature dependence of the thermal response ΔT in good agreement with the expected Kapitza conductance behaviour ($\Delta T \propto T_{bath}^{-n}$, $3<n<4$). Moreover the n-exponent is not dependant on the heat power, as it was in the case of the "epoxy" thermometers.

Fitting experimental results with numerical modelling data, allow us to estimate the Kapitza conductance. The obtained values are in good agreement with the previous results reported by several authors using a different measurement method.

The "vacuum" thermometers are currently used on the TE011 mode cavity with Nb and NbTiN plates and the first results are presented.

1. SURFACE THERMOMETRY IN SUPERFLUID HELIUM

Superconducting cavities in the frequency range 1.5 GHz - 3 GHz begin to be widely applied for high energy electron accelerators. This frequency range imposes Superfluid Helium (Helium II) as cooling medium with working temperature between 1.8 K and 2 K.

Development of diagnostic techniques for SC cavities is tightly connected to the continuous effort to improve the performance of these resonators in two directions: a) increasing the accelerating gradient E_{acc}, b) increasing the quality factor Q_o.

Surface temperature measurements of the helium cooled side of the cavity wall is a classical diagnostic technique which has seen major improvements in the last five years . This technique is progressively moving from a "qualitative" approach (mapping techniques for coarse detection of defect points and quench related heating) toward the development of "quantitative" devices able to measure surface temperature with sufficient accuracy and reproducibility. Studies on local surface residual resistance and electron emission characterization are two important topics where accurate thermometry can contribute to enhanced insight into these phenomena which currently limit cavity performance.

The electromagnetic field in an accelerating cavity generates thermal power losses per unit area q_s, proportional to the local surface resistance R_s :

$q_s = 1/2 \, (R_s \, . \, H^2)$ where H is the peak magnetic field at the surface.

Considering the case of a homogeneous surface with constant R_s, heated by a uniform magnetic field (no radial heat diffusion), the temperature jump ΔT across the metal - Helium II interface ($\Delta T = T_{wall} - T_{bath}$) is simply related to q_s by :

$\Delta T = q_s / H_k$ where H_k is the Kapitza conductance (for $T_{bath} < 2.17$ K)

In the case of Electron Field Emission, electrons accelerated by the electromagnetic field impact the cavity wall with high energy (500 keV - 2 MeV) and currents in the nA - μA range. From a given emission site, according to the Fowler - Nordheim theory of field emission from a metal surface, combined with the field map of the cavity, the electron trajectories can be easily calculated and consequently, the heat

flux density distribution created by the impacting electrons. The resulting temperature jump ΔT can be related to the heat flux density as previously stated.

Due to the high effective thermal conductivity of Helium II, the temperature difference of the cavity wall with respect to T_{bath} , on the liquid side is largely dominated by the solid/Helium II interfacial temperature jump ΔT , controlled by Kapitza conductance ($\Delta T / \Delta T_{bath} \cdot 10^6$). Furthermore the temperature profile decreases sharply in the thin boundary layer near the solid surface : thickness - **15 Å** at T_{bath} = **1.8 K** [Roberts and Donnelly 1974] . Consequently measuring the surface temperature is a difficult task which presents two major requirements for the surface temperature sensor: very good thermal contact with the cavity wall and very efficient thermal insulation from the surrounding Helium II bath.

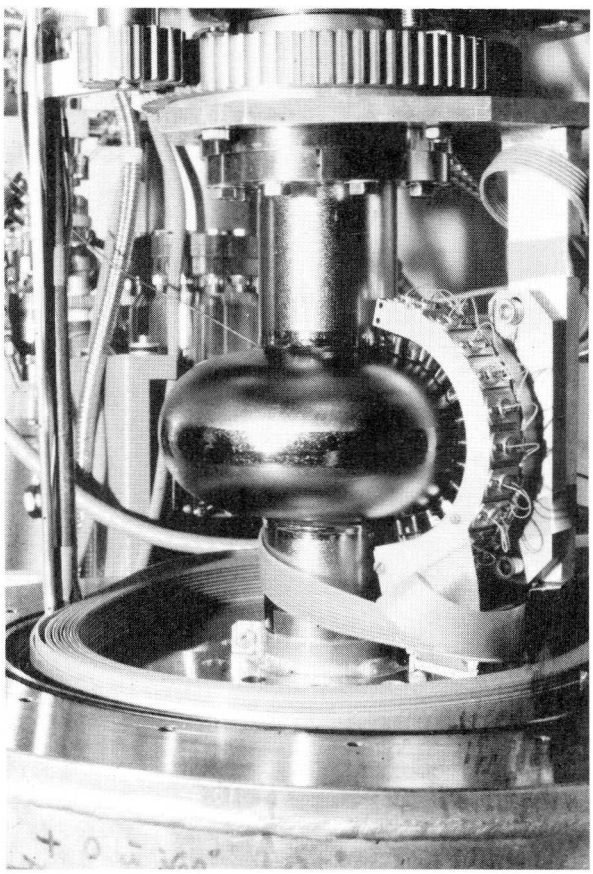

Fig 1 : Scanning arm for monocell 1.5 GHz cavities

The first steps to solve these difficulties where taken at Cornell Univ. [Muller, Kneisel 1985] where the first surface thermometers were developed and applied to surface resistance studies. High speed thermometry was also developed at this laboratory [Padamsee, Reece 1987] for electron emission studies in monocell cavities at 1.5 GHz.

At the GECS laboratory, following an idea of Dr. Muller from Wuppertal Univ. and in close collaboration with them, a special thermometer was developed for use on a scanning arm (Fig. 1) mounted on monocell 1.5 GHz cavities [Aune et al. 1988].

This scanning arm carries 13 thermometers placed along a meridian line of the cavity with a spacing of 11 mm. Electronic circuits control the movement in synchronization with the pulsed RF power. The start angle, the

end angle and the step amplitude (≥ 1°) can be programmed. After some improvements, the use of this diagnostic tool has become routine for all the tests with monocell cavities. A typical temperature map is shown in Fig. 2, along with the X - ray map obtained with a Si-diode array placed on a separated rotating arm at a meridian line 90° away from the thermometer array. An electron trajectory impact is clearly observed along a meridian in the temperature map, which is perfectly correlated with the X - ray map.

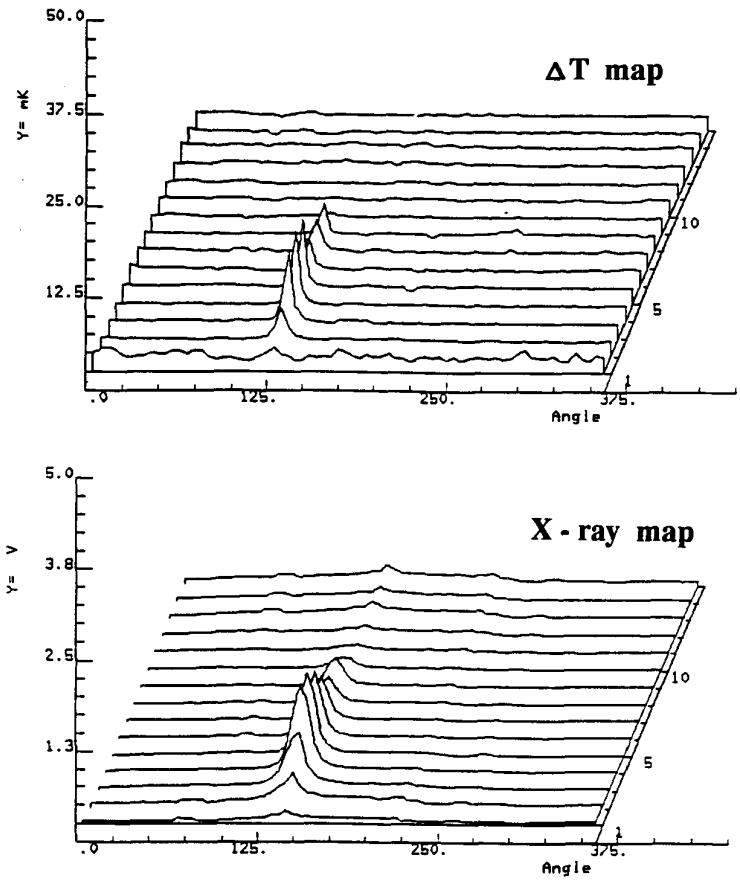

Fig. 2 : Temperature and X-ray maps of a 1.5 GHz monocell cavity.

T_{bath} = 1.5 K E_{acc} = 22 MeV/m

Several interesting anomalous loss effects have been observed with this scanning system. Typically these involve heating due to electron emission, however in several cavities quench regions located near the equator have been clearly identified. The origin of the quench is not yet well understood , and no appreciable heating was detected in the quench area at field level just below the cavity breakdown.

It must be stressed here that the thermal response of the scanning thermometers as a function of the heat flux density (i. e. ΔT vs. q_s) is non-linear and depends in a complicated way on bath temperature. This behavior is principally due to the bad thermal contact between the sensor tip and the cavity wall (no thermal bonding agent is used). Moreover, this scanning thermometer cannot be calibrated with sufficient accuracy for quantitative analysis of anomalous losses in the RF surface.

The large number of temperature maps resulting from systematic tests of monocell cavities along with numerical model calculations allow us to evaluate the measurement efficiency η of this kind of thermometer :

$$\eta = \Delta T \text{ (measured)} / \Delta T \text{ (Kapitza)}$$

$$1\% < \eta < 3\%$$

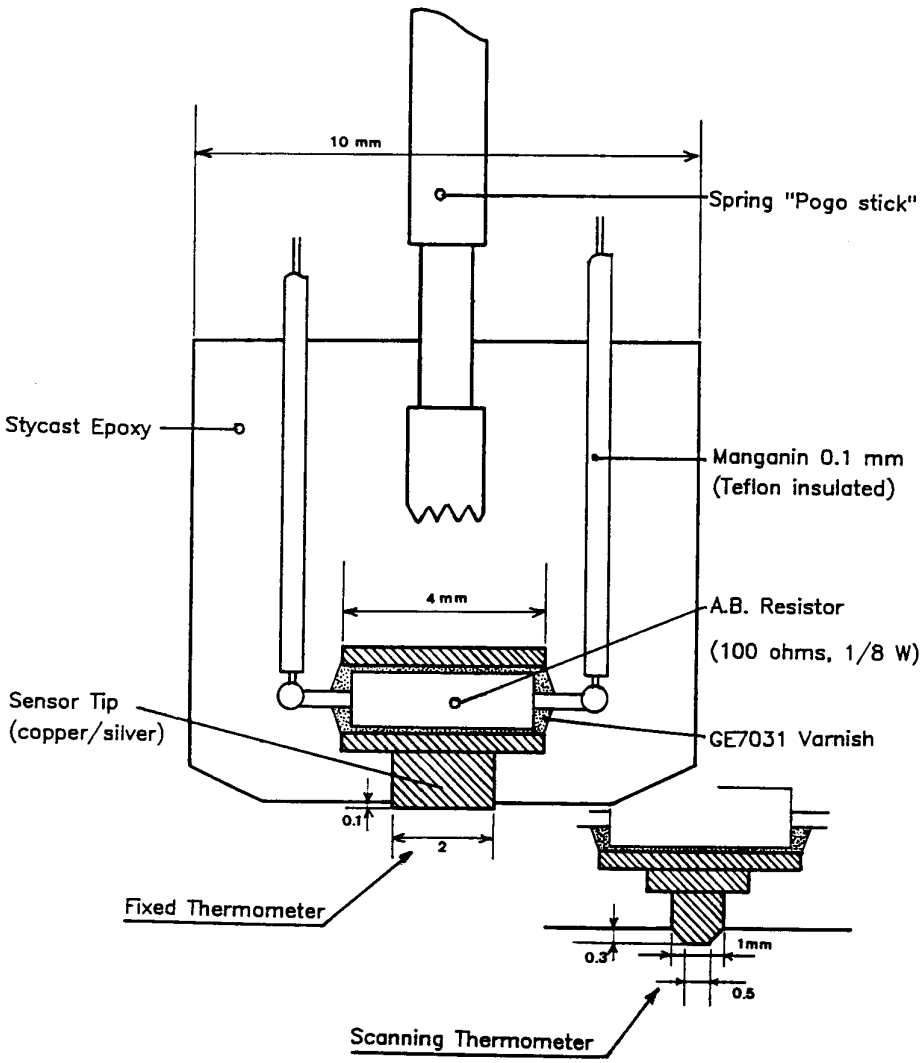

Fig. 3 : Cross-section of an epoxy thermometer

This poor efficiency appears to be inherent to the thermometer structure and in particular its poor thermal contact with the cavity wall. Further improvements of this scanning model were undertaken in order to develop a fixed thermometer of higher sensitivity for surface resistance studies in a TE011 mode cavity. The main difference of this new design compared with the scanning thermometer, was the sensor tip diameter of 2 mm which is well polished and adjusted to stick out from the epoxy body by a length of 0.1 to 0.2 mm (Fig. 3). This sensor is held in contact with the niobium wall by mean of a spring and Apiezon N grease or GE7031 varnish is used as a thermal bonding agent.

In order to estimate the efficiency ot the "epoxy" thermometer, a numerical model of the thermometer incorporating the calibration cell was performed. Experimental data and numerical results where compared with good agreement [Brizzi et al. 1990], leading to a mean efficiency $\eta = 30\%$. Reproducibility and interchangeability better than **70%** were obtained, after thermal cycling between 4.2 K and 300 K and a sensor mounting / demounting sequence. The reproducibility was essentially limited by the mechanical and contact mounting conditions at the Niobium plate - sensor tip interface. According to this study, two relevant conclusions can be outlined:

1) This non-adiabatic "epoxy" thermometer, connected to the two different temperatures T_{wall} and T_{bath}, modifies the cooling conditions of the Niobium wall at the sensor location. It induces a local temperature perturbation on the Niobium wall. In addition the finite heat flow traversing the sensor, creates a temperature gradient inside the sensor itself, thereby reducing the measurement efficiency.

2) The bath temperature dependence of the thermometer thermal response is far from the expected behaviour controlled by the Kapitza conductance ($\Delta T \propto T_{bath}^{-n}$ with $3 < n < 4$). Values of n in the range $2 < n < 13$ were observed during the tests. All this confirms the non-adiabatic behavior of the sensor and the bad thermal link to the Niobium wall. Heat flux crossing the interface area between the sensor tip and the cavity wall, where Helium II microscopic channels can be formed inside the thermal bonding agent, can modify to a large extent the bath temperature dependence of the thermometer response. The effective thermal conductivity k_a of Helium II in narrow capillaries in subcritical regime [Fouaidy 1989] is strongly temperature dependent ($k_a \propto T^{12} \cdot d^2$, where d is the channel diameter). Moreover, the heat transport properties in these Helium II capillaries change, with increasing heat flux density, to a non-linear regime [Gorter and Mellink 1949]. Thus, on dimensional grounds, the large value of the n exponent can be explained in terms of an overall thermal conductance modification in the sensor / bonding agent / cavity wall sandwich.

2. ACCURATE CALIBRATION OF EPOXY THERMOMETERS

2.1 Experimental set-up and measurement procedure

A special calibration cell simulating RF surface heating in a cylindrical TE011 mode cavity (4 GHz) which is used to investigate spatial resistance distribution on various SC removable endplates [Juillard et al. 1990], has been designed. This calibration assembly (Fig. 4) allows us to perform accurate calibration measurements which include the study of reproducibility, interchangeability and dispersion, of the 40 fixed "epoxy" thermometers array.

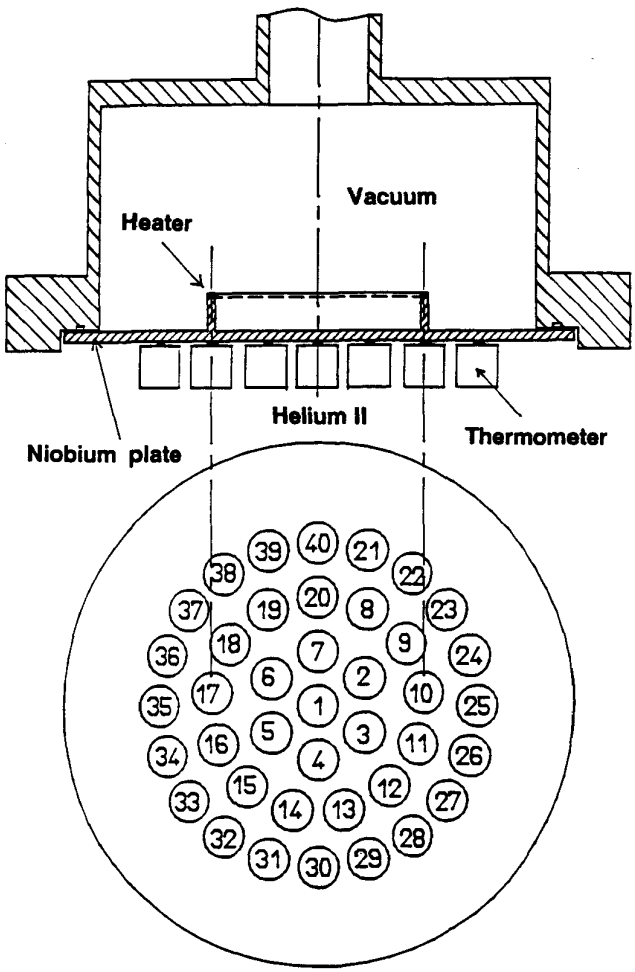

Fig. 4 : Calibration assembly for the 40 epoxy thermometer array

Two test assemblies (plate and heater) have been used during the calibration experiments. Both were machined from reactor grade Niobium ingots (**RRR=32**). The heater is simply a manganin wire (**diameter = 0.1 mm** and **R=100 Ohms**) wrapped inside a groove located at the radius **r = 26.4 mm** of the Niobium plate. This heater location corresponds exactly to the maximum surface magnetic field in the TE011 cavity, where 13 fixed thermometers are located on the Helium II cooled side. Before calibration the Niobium specimen is treated following the standard GECS chemical and surface preparation procedures [Aune et al. 1990] in order to reproduce the same surface state as in the TE011 cavity, and hence, the same Kapitza conductance.

The test specimen is placed in a stainless steel vacuum can. Particular attention was attached to the heat power measurement and control : a high stability power supply and four-lead measurement circuitry were used. The length and diameter

of the copper leads connecting the heater to the vacuum feedthrough were chosen in order to reduce joule heating and conduction heat leaks (**< 1%**) to the surrounding Helium II.

The bath temperature which is measured by a calibrated Germanium thermometer (Lake Shore type GR-200B-500) is controlled to within **± 0.15 mK** for T_{bath} **< 2.17 K** , for heat loads as large as **500 mW** by regulating the Helium vapor pressure (MKS pressure transducer and valve controller).

The resistance changes $R_i(T_{bath})$ of the sensors (40 thermometers), are measured by the four-lead technique using a high stability (10^{-4}) DC current source. This current, which is adjusted according to the bath temperature, so as to achieve low and constant self heating ($\simeq$ **0.2** μ**W**) of the sensors is monitored via the voltage drop across a precise 100 kOhms resistor. The sensor current is reversed at each measurement in order to eliminate thermal voltages ($\approx$ **5** μ**V**). The resistance measurement is performed by a scanning technique using an HP44705 relay multiplexer and an HP3458 voltmeter leading to an overall resolution of **1 - 2** μ**V** which corresponds to **20** μ**K at 1.5 K**. The precision of ΔT measurements, which is limited by the bath temperature regulation system, permits the detection of minimum RF losses of roughly **10** μ**W**. All the sensors are resistance calibrated, **R(T)** , in situ at zero power, using the Germanium sensor as reference thermometer, and a least square fit yielding the coefficients of the expansion:

$$\frac{1}{T} = \sum_{i=0}^{n} a_i (\mathrm{Log}(R))^i \qquad \text{with} \qquad n = 2$$

The power calibration (ΔT vs. **P** , where **P** is the heater power) is performed by comparing the **i-th** sensor temperature deduced value T_i to T_{bath} which is given by the Germanium thermometer, at zero and finite heater power. The final temperature jump ΔT_i at the surface is obtained from the formula :

$$\Delta T_i = (T_i(P) - T_{bath}(P)) - (T_i(0) - T_{bath}(0)) .$$

This method minimizes errors from residual calibration inaccuracies (fit and precision) or possible $R_i(T)$ shifts between the resistance - temperature calibration and the temperature - power calibration experiments.

2.2 Experimental calibration results and discussion

A typical thermal response of 40 fixed epoxy thermometers array is presented in Fig.5 . Apiezon N grease is used as thermal bonding agent between the sensor tip and the Niobium test plate with a contact pressure of 6 bars. At T_{bath} = **1.62 K** and **P = 246 mW**, a good mean sensitivity **ΔT = 39.2 mK** is obtained for the thirteen thermometers (# 8 to # 20) located at the opposite side of the heater.

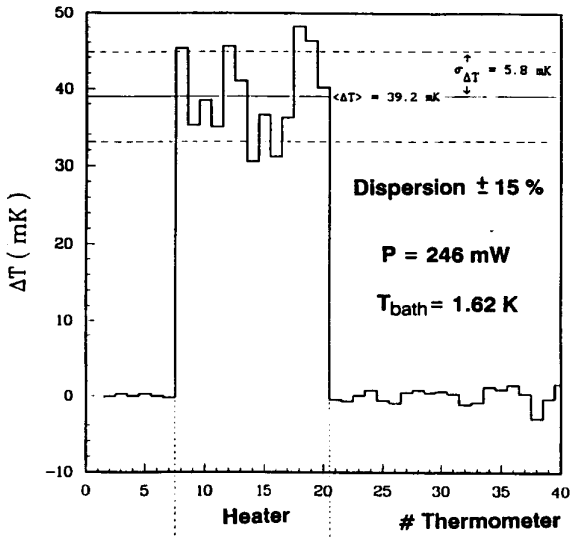

Fig. 5 : Thermal response of the epoxy thermometer array

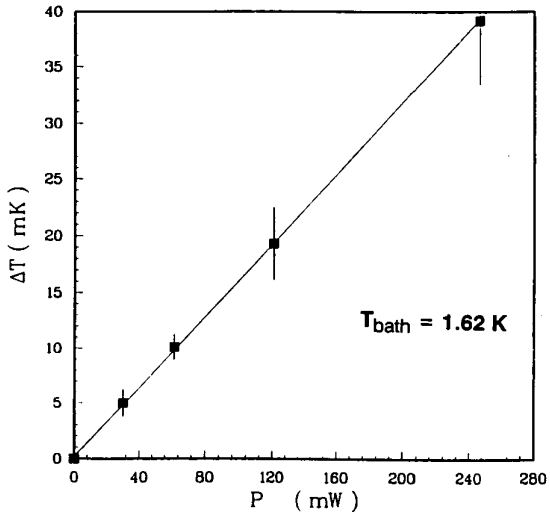

Fig. 6 : Mean thermal response

The dispersion (± **15%**) is quite good for this system, confirming our earlier results [Brizzi et al. 1990] on the calibration of individual thermometers. This dispersion seems certainly to be linked to thermometer mounting (positioning and contact pressure). As expected the dispersion increases with bath temperature (± **30 %** at T_{bath} = **1.84 K**), due to the strong T_{bath} dependence of the **ΔT** response : $\Delta T \propto T_{bath}^{-8.2}$. The mean thermal response of the thirteen thermometer group measured at 1.62 K (Fig. 6) shows a good linearity in the power range corresponding to studies on RF losses in Niobium cavities (i.e. at 4 GHz a "bad" Niobium plate with R_s = **300 nOhm** exposed to a magnetic induction of **500 Gauss** can generates heat flux densities of **24 mW/cm²**).

2.3 Numerical simulation of a TE011-like calibration cell

A precise simulation of the test cell was needed to estimate the efficiency of fixed epoxy thermometers. Due to the geometry of the Niobium sample and the heater

location, this problem cannot be handled by using simplified codes [Padamsee 1982] [Tuckmantel 1984] . It was thus necessary to develop a more elaborate computer code for this purpose.

The POISNL computer code was developed in our laboratory for steady state heat transfer simulations using the MODULEF package (Software Library of Finite Element MODULEs . [Bernardou et al. 1988]) . This code solves the non-linear steady state heat equation , with the appropriate boundary conditions, in cylindrical coordinates (**r , z**) for a 2D - axisymmetrical calculation domain :

$$\frac{1}{r}\frac{\partial\left(rk_i(T)\frac{\partial T}{\partial r}\right)}{\partial r}+\frac{\partial\left(k_i(T)\frac{\partial T}{\partial z}\right)}{\partial z}+\sigma_i=0$$

where $k_i(T)$ is the thermal conductivity of the i^{th} - medium (subdomain) and σ_i is the rate of heat generation per unit volume inside this subdomain. For the most part of problems concerning RF superconductivity thermal effects, there is no heat generated inside the superconductor (i.e. $\sigma_i = 0$) .

The problem has to be solved with the following boundary conditions (Fig.7)

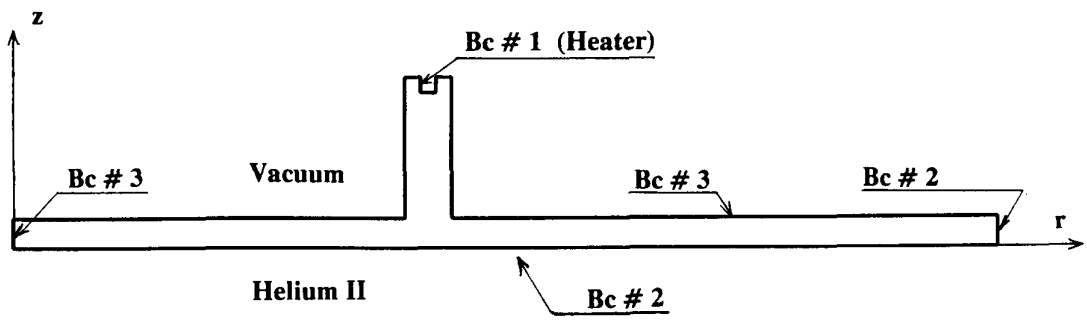

Fig. 7 : Boundary conditions of the TE011-like cell

Boundary condition # 1 : At the heater location, the Niobium sample is subjected to an uniform heat flux density **q**

$$q=\frac{P}{\pi Dl}=k(T)\left(\frac{\partial T}{\partial r}\right)_{r=r_0}\quad\text{for}\qquad z_0\le z\le z_1$$

where $l = z_1 - z_0$ is the height of the heated region (manganin wire location)

Boundary condition # 2 : On the Helium II cooled side of the Niobium plate, as well as at plate rim, the heat transfer is controlled by Kapitza conductance H_k ,

a) on the Helium II wetted side of the plate :

$$k(T)\left(\frac{\partial T}{\partial z}\right)_{z=0} = H_k.f_e(\Delta T).(T - T_{bath}) \qquad \text{for} \qquad 0 \le r \le r_0$$

b)on the Helium II wetted rim :

$$-k(T)\left(\frac{\partial T}{\partial r}\right)_{r=r_0} = H_k.f_e(\Delta T).(T - T_{bath}) \qquad \text{for} \qquad 0 \le z \le e$$

where r_0 and e are the Niobium plate radius and thickness respectively.

$H_k = h_0 \cdot T_{bath}^{\,n}$ is the Kapitza conductance at the Niobium / Helium II interface for moderate heating (i.e. $\Delta T << T_{bath}$), h_0 and n are constants depending on surface state which are experimentally determined and discussed in the following.

$$f_e = 1 + \frac{3}{2}\left(\frac{\Delta T}{T_{bath}}\right) + \left(\frac{\Delta T}{T_{bath}}\right)^2 + \frac{1}{4}\left(\frac{\Delta T}{T_{bath}}\right)^3$$

$$\text{with} \qquad \Delta T = T - T_{bath}$$

is an enhancement factor correcting H_k for "high" heating ($\Delta T > 0.1\ T_{bath}$) corresponding to the complete expansion of the formula :

$$\frac{(T^4 - T_{bath}^{\,4})}{4T_{bath}^{\,3}\Delta T}$$

according to the black body Debye phonon radiation theory.

Boundary condition # 3 :

a) True adiabatic wall (i.e. no heat leaks to the surrounding)

b) Fictitious adiabatic wall (symmetry)

$$k(T)\left(\frac{\partial T}{\partial r}\right)_{r=0} = 0 \qquad \text{for} \qquad 0 \le z \le e$$

the radial component of the heat flux density is vanishing on the Niobium sample **z** - axis.

A close view of a typical POISNL result is presented in Fig. 8 , showing the isotherms inside the test specimen. Two input data are needed for this purpose: the thermal conductivity **k(T)** which was measured separately at the GECS laboratory [Koechlin 1991] using test samples machined from the same Niobium ingot (**RRR = 32**), and the Kapitza conductance H_k **= 0.2 W/cm².K** at T_{bath} **= 1.6 K.** This value was deduced from the measurements with vacuum thermometers, discussed in Section **3.3.**

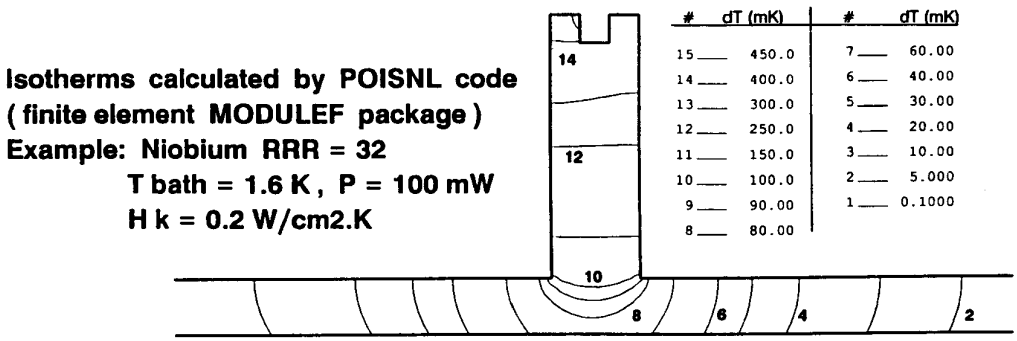

Fig. 8

The isotherms in the lower side of the heater wall , near the plate, are planes perpendicular to the wall, and the heat flux density is uniform and well defined in this region. The radial heat diffusion begins immediately at the bottom of the heater wall.

The results obtained with this model are strongly dependent on the Kapitza conductance value. The **ΔT** jump at the interface, was calculated using two different values of the Kapitza conductance (at T_{bath} **= 1.7 K** and **P = 100 mW**) :

[Mittag] $H_k = 0.017 \cdot T_{bath}^{3.62} \cdot f_e(\Delta T) = 0.116\ W/cm^2K$ --> **ΔT = 53.4 mK**

[IPN-GECS] $H_k = 0.043 \cdot T_{bath}^{3.18} \cdot f_e(\Delta T) = 0.230\ W/cm^2K$ --> **ΔT = 33.6 mK**

In this example, a factor of **2** on the H_k value, leads to a **1/1.6** factor on the temperature jump **ΔT**.

2.4 Surface Temperature Measurements in a TE011 cavity

The cylindrical cavity, resonating at TE011 (4 GHz) and TE012 (5.6 GHz) modes, was constructed in order to study the RF surface resistance $\mathbf{R_s}$ of different bulk and film superconductor samples [Juillard 1990] . The cavity was made out of high purity Niobium (**RRR = 180**) with a removable end plate of **126 mm** external diameter. The inner diameter of the cavity is **110 mm** and the height is **66 mm** .

Forty epoxy thermometers are mounted on the Helium II cooled side of the plate . Fig. 9 shows the mechanical set up of the thermometer array which provides easy positioning and pressure adjustement .

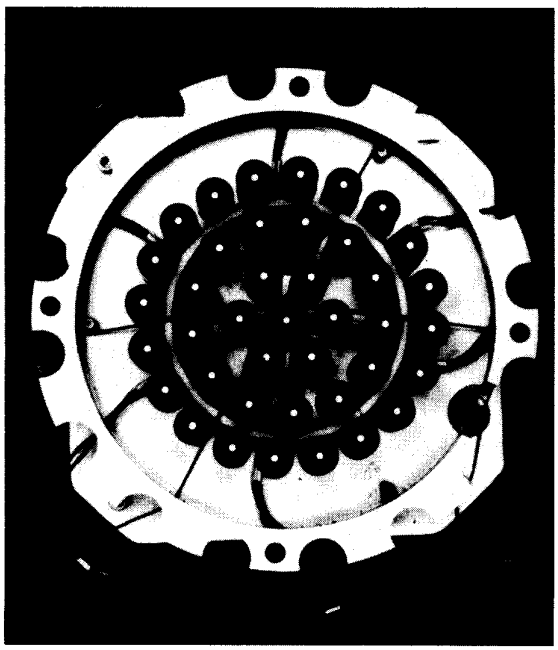

Fig. 9 : Epoxy thermometer array

These fixed thermometers are distributed over the plate on several concentric circles of radius **r** corresponding to different surface magnetic induction values :

#1 at the end plate axis
#2 ..#7 at **r = 12.7 mm, B = 0.69 B_{max}**
#8 ..#20 at **r = 26.4 mm, B = B_{max}**
#21..#40 at **r = 39.1 mm, B = 0.74 B_{max}**

where $\mathbf{B_{max}}$ is the maximum surface magnetic induction on the endplate in the TE011 mode of the cavity.

During the last 18 months, a large number of tests were performed with different end plate samples. For bulk Niobium, typical mean $\mathbf{R_s}$ values were measured with good reproducibility in the range of **50 nOhms** to **150 nOhms** (measured at low field, for **1.6 K < T_{bath} < 1.7 K** , and **f = 4 GHz**). The magnetic induction was limited, for these tests, to a maximum value of **500 gauss** by a quench, which seems to be independent of the end plates, and could possibly be caused by enhanced losses at the upper plate of the cavity. Nevertheless, it is possible to explore a reasonably large range of magnetic fields with this cavity.

From the thermometry point of view, we can outline the following surface temperature measurements and interesting related observations :

a) Temperature maps of bulk Niobium end plates

Fig. 10 shows a typical temperature map of a Niobium end plate (**RRR = 180**), with several apparent hot points.

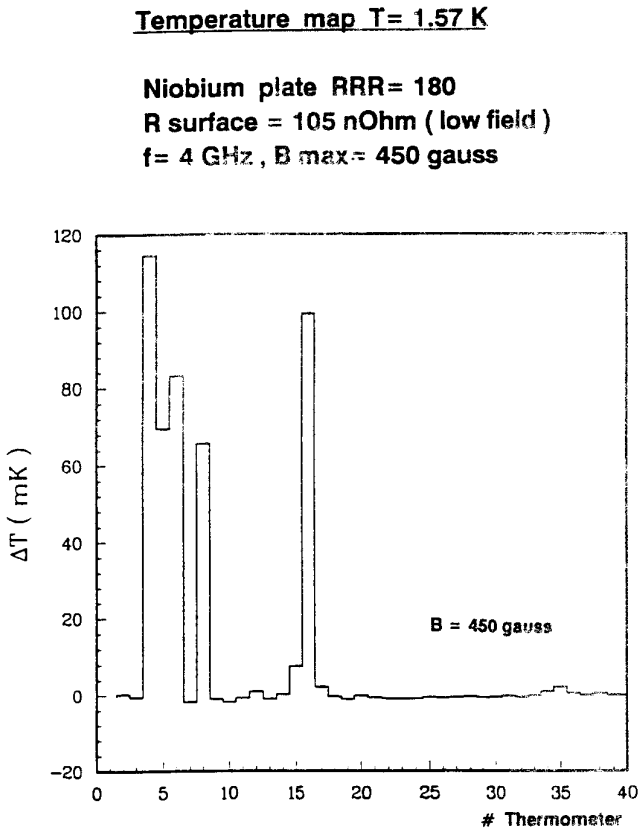

Fig. 10

In this experiment the magnetic induction was limited by a quench at **B = 500 gauss**. RF measurements gives a surface resistance of the end plate R_s **= 105nOhms** at low field, increasing slowly with the field (R_s **= 240 nOhms** at **B = 475 gauss**). The thermal response of several thermometers was studied in more detail, as a function of the peak max. magnetic induction on the plate (**ΔT vs.** B_{max}). A power law fit was adopted ($\Delta T \propto B_{max}^{n}$) in order to compare the respective results. Two major features have been observed :

1) Thermometers sensing small heating ($\Delta T \leq$ **10 mK** in the range $0 < B_{max} < 500$ **gauss).** In this case the fit gives an exponent : $2 < n < 4$.

2) For high heating (corresponding to the five hot points of the Fig10), the fit gives an exponent : $5 < n < 7.5$

More precise measurements were made on two thermometers showing a low heating (**#11** and **#12**). This time a sensitive analog recorder was employed to visualize and measure **ΔT** simultaneously with the bath temperature drift, so as to improve the measurement precision. The **n**-exponent for the two thermometers was estimated by fitting to the power law :

$$n = 3.7 \quad \text{for} \quad 0.25\ \text{mK} < \Delta T\ (\#\ 11) < 1.55\ \text{mK}$$
$$n = 3.55 \quad \text{for} \quad 0.2\ \text{mK} < \Delta T\ (\#\ 12) < 0.84\ \text{mK}$$

b) Low surface resistance sample

An interesting result was obtained with another bulk Niobium end plate having a very good R_s value (R_s = **50 nOhms** at T_{bath} = **1.6 K** and **f = 4 GHz**), nearly constant over the whole magnetic induction range (**0 - 500 gauss**).

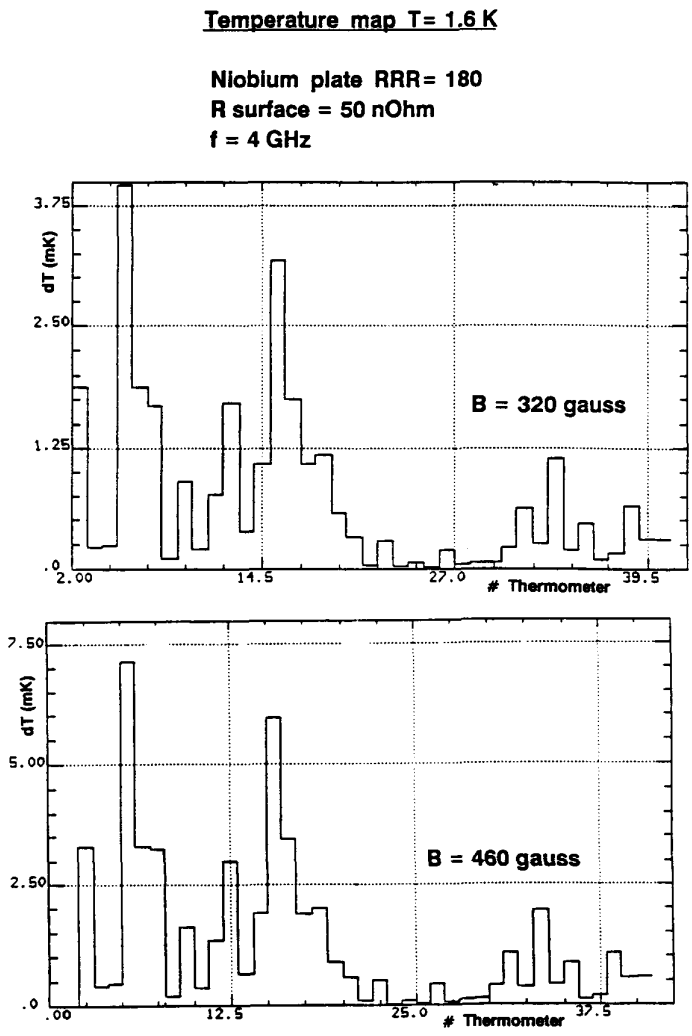

Fig. 11

This time the temperature map (Fig. 11) does not shows any important heating of the surface, even at high field : $\Delta T_i < 10$ **mK** for the whole thermometer array. The equivalent background noise observed during the experiment, at zero magnetic field, was very low (± **50** μ**K**) . Fig. 11 displays two complete maps of the end plate at two different magnetic induction levels : B_1 = **320 gauss** and $B_2 = \sqrt{2} B_1 = 460$ **gauss**. It can be observed that the two maps are perfectly homothetic and the majority of thermometers fit well the expected result :

$$\Delta T_i(B_2) \approx 2\,\Delta T_i(B_1)$$

which confirms the general surface temperature heating trend : $\Delta T_i \propto B^2$.

c) NbTiN film sample

More recently, sputtered NbTiN films coated on a copper surface have been tested on the TE011 cavity. The surface resistance of these samples , R_s **> 400 nOhms** (at low field) for the best samples, is larger than the value usually measured with the bulk Niobium samples. The NbTiN sample used for thermometry measurements have a rather high surface resistance R_s **= 4300 nOhms** (at low field , T_{bath} **= 1.7 K ,** **f = 4 GHz**) increasing strongly with the field (R_s **= 33800 nOhms** at **B = 190 gauss**) . The strong dependence on **B** is thought to be mainly related to thermal effects linked to the very high R_s values. This experiment gives a good means of testing the linearity of the thermometer thermal response . Fig. 12 shows the plot of local ΔT corresponding to several thermometers sensing significant heating , as a function of the heat flux density q_s :

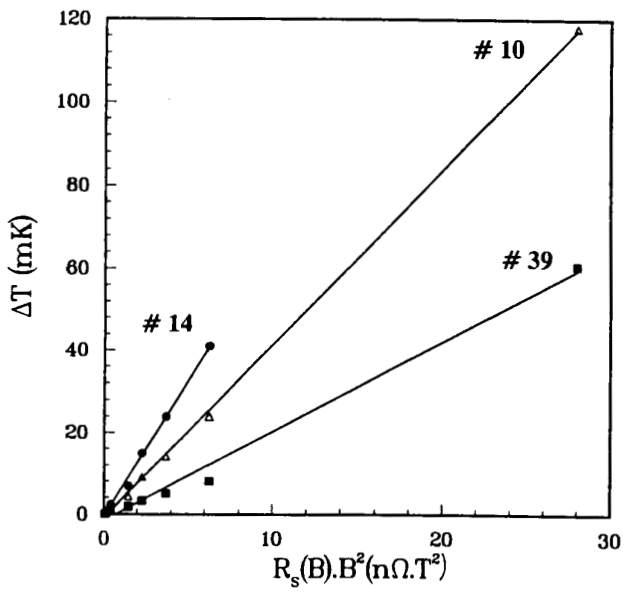

Fig. 12 : Temperature measurements on a NbTiN sample

$$q_s \propto R_s(r,B).B^2$$

$R_s(r,B)$, the local surface resistance which depends on the local magnetic induction at **r** radius, is not accessible by direct measurement, but it may be deduced from the relation $\langle R_s \rangle = f(\langle B \rangle)$, where $\langle R_s \rangle$ is the total surface resistance of the sample resulting from Q_o measurements, and $\langle B \rangle$ is the mean surface magnetic induction calculated by integrating the field distribution over the plate surface . **B** is the magnetic field at the thermometer location.

3. VACUUM THERMOMETERS

The previous experimental study together with numerical simulation leads to a mean "epoxy" thermometer efficiency of **30 % ± 10%** , if the interchangeability and reproducibility after mounting / dismounting sequence and thermal cycling (4.2 K - 300 K) are included. Consequently, these thermometers are inadequate for an accurate study of the heating effects of the RF surface resistance distribution (TE011 cavity). Numerical simulations show that this low efficiency can be principally attributed to the poor effectiveness of the thermal insulation of the thermometer epoxy housing. Furthermore the efficiency of an ideal reference thermometer of the same geometry as the epoxy thermometers, but with the epoxy housing replaced by an adiabatic wall, reaches **90 %** in simulations. On the basis of this numerical study a new type of thermometer with an improved efficiency has been developed.

3.1 Description of vacuum thermometers

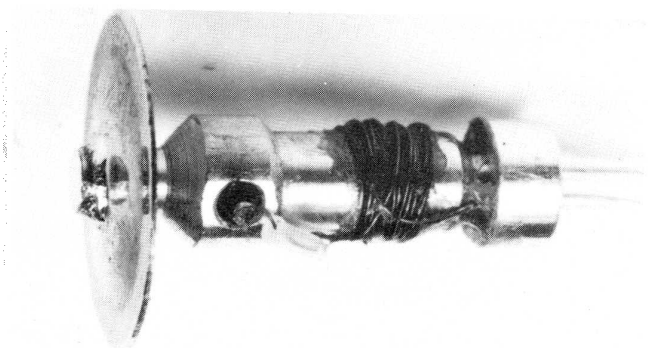

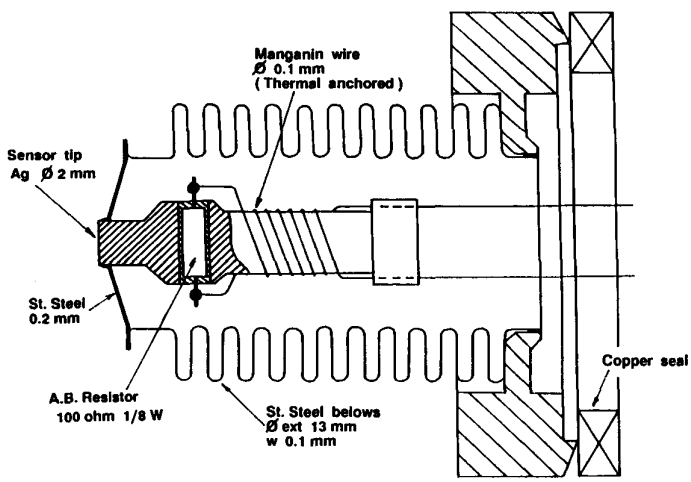

Fig. 13 : Cross section of a vacuum thermometer

The design of these "vacuum" thermometers was performed taking into account several main requirements : small size, low conductive heat leaks, reliability and easy of manufacture.

The thermal insulation of the thermometer against Helium II has been drastically improved, as compared to "epoxy" thermometers, by placing the sensor in a small vacuum jacket. A cross-sectional view of the thermometer is shown on Fig. 13. The sensitive part of the thermometer is an Allen-Bradley (AB) carbon resistor (100 Ohm , 1/8 W) housed in a silver block with a sensor

tip for thermal contact with the Niobium wall. The AB resistor, with the bakelite protection ground off, is glued to its housing with GE7031 varnish. Manganin wires of 0.1 mm diameter and 40 cm length, thermally clamped to the silver housing over 10 cm, are used as electrical leads connecting the sensor to the feedthrough. In the worst case (i.e. bad thermal clamping of the sensor leads) the heat conduction leaks are still much lower than joule heating of the sensor. The sensor tip is Electron Beam (EB) welded to a bottom flange made from a stainless steel thin sheet (diameter 10 mm, thickness 0.2 mm) . The Helium II wetted part of the sensor tip is machined to protrude only 0.1 mm from the stainless steel can, in order to reduce heat leaks to the Helium II bath. A stainles steel bellows (thickness 0.1 mm) is EB welded to the bottom flange for positioning and control of the contact pressure (**30 - 100 bar**) between the sensor tip and the Niobium wall. This bellows together with the flange constitutes the vacuum insulating jacket of the sensor. First prototypes have been equiped with standard stainless steel vacuum flanges (copper seals) at the upper part of the sensor and connected to the same pumping line as the calibration cell.

3.2 Experimental cell and measurement procedure

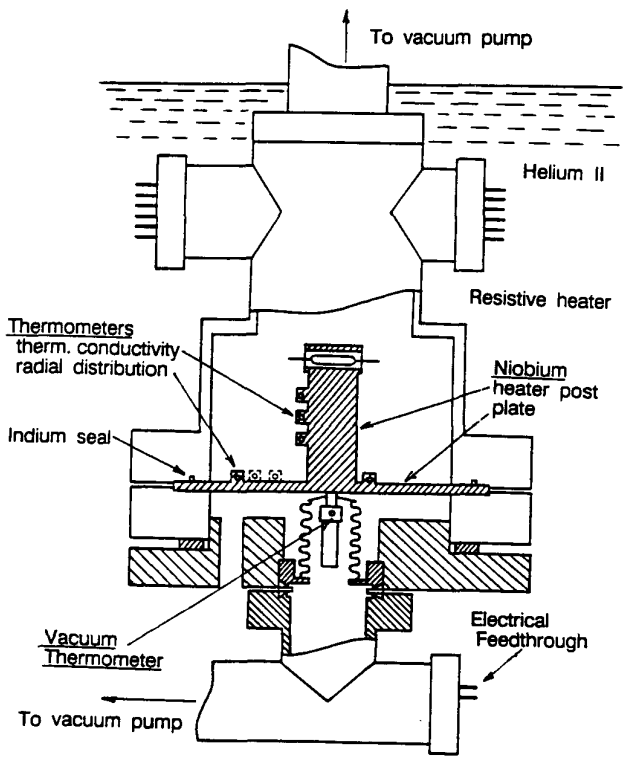

Fig. 14 : Vacuum thermometer test cell

The test cell (Fig. 14) has been significantly improved as compared to the previous one used in our first calibrating set-up [Brizzi et al. 1990]. The Niobium plate - heater post assembly was machined from a high purity Niobium ingot (**RRR=270**) supplied by Wah - Chang, in order to avoid unknown thermal contact resistances due to gluing and discontinuities in thermal conductivity.

This test assembly is placed in a stainless steel vacuum insulated can. Heater power is supplied by mean of a resistor (**R = 40 Ohm**) placed in a hole at the top of the heater post, and bonded with Stycast. Three AB resistors are located in special holes at the periphery of the heater post,

separated by **Δz = 4.5 mm** , in order to perform an accurate measurement of the Niobium thermal conductivity. Four other AB resistors, installed in special housings machined into the heated side of the Niobium plate at different radii (**r_1=7.7 mm, r_2=11.7 mm, r_3=15.7 mm, r_4=19.7 mm**) are used to measure the radial temperature distribution. Four manganin wires of 40 cm length, thermally clamped to metal supports so as to reduce perturbating heat leaks, were used for all these thermometers.

The "vacuum" thermometer under test was installed at the center of the Helium II cooled side of the Niobium plate. A spacer of well defined thickness between the bottom flange of the test chamber and the mounting support of the thermometer, together with the thermometer bellows, allow us to adjust the contact pressure to the desired value (**30 - 100 bar** at room temperature). Thermal contact between the sensor tip and Niobium plate is improved by the use of a bonding agent : Apiezon N grease. In this experiment, the data acquisition system is based on Keithley solid state multiplexers and a high precision Keithley Nanovoltmeter. The overall accuracy was, like the system used for "epoxy" thermometers, limited by the bath temperature regulation system **(±0.15 mK)** .

3.3 Results and discussion

Experimental results

The thermal response **ΔT = f(P)** of the two types of thermometer , "epoxy" and "vacuum" , at different bath temperature are compared in Fig. 15 :

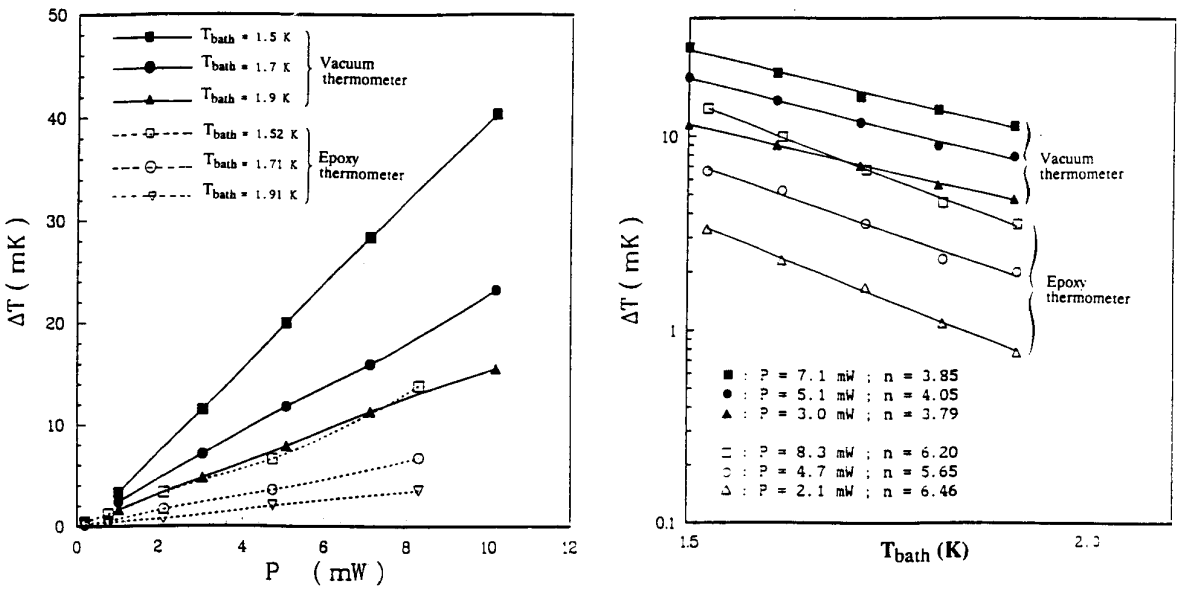

Fig. 15 : Thermal response of epoxy and vacuum thermometers

The "vacuum" thermometer response curve shows a good linearity and improved sensitivity by a factor of **2.5 to 4.4** , depending on bath temperature, as compared to "epoxy" thermometers. Note that the relative efficiency increases with T_{bath} due to a stronger bath temperature dependence of the "epoxy" thermometers. In the range of heater power studied ($P \leq 10$ mW) , the mean **n** - exponent values in the bath temperature dependence expression $\Delta T \propto T_{bath}^{-n}$, are **3.9 ± 0.1** and **6.4 ± 0.3** for vacuum and epoxy thermometers respectively. The expected sensitivity enhancement is attributed to the following two factors : improved thermal contact to the Niobium plate (the contact pressure has been increased by a factor ≥ 4), and the reduced thermal link to the Helium II (adiabatic wall and low conduction heat leaks) .

The **n** - exponent value is a good criterion for evaluating the quality of Helium II wetted surface temperature measurement. A good measurement must lead to a T_{bath} effect controlled by the Kapitza resistance. We can then conclude that "vacuum" thermometers, in contrast to "epoxy" thermometers, measure a surface temperature closer to the true one : the **n** - exponent values are within the range of those obtained by other authors ($3.62 \leq n \leq 4.65$) using different experimental arrangement [Mittag 1973] [Wilkes 1978].

Finally, the contact pressure effect on the "vacuum" thermometers thermal response has also been studied : three pressure values were used (30 bar, 60 bar and 90 bar), but no clear systematic effect was found. This may be caused by a possible variation of the Niobium state surface, and consequently Kapitza conductance variation between different runs. The pressure is modified by changing the thickness of a spacer in the experimental cell, this imposes warming cycles to room temperature and exposures to the atmosphere for long periods. A special arrangement is planed for in situ continuous pressure adjustment.

Model calculations

The experimental cell (Fig. 14) has been designed with three purposes in mind : accurate calibration of thermometers including efficiency estimate, measurement of Kapitza conductance of Niobium specimens with the same surface preparation as for SC cavities, and finally experimental validation of the POISNL code. This code has already successfully passed several tests by comparing the numerical results to an analytical solution and to different numerical data obtained from other computer codes : the

mean standard deviation using the analytical solution as reference was less than 1 % for all the tested codes [Fouaidy 1990].

The boundary conditions of the experimental cell are represented in Fig. 16 :

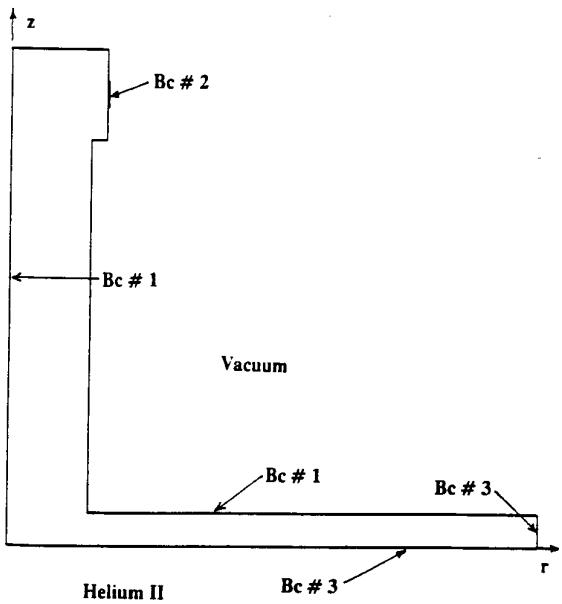

Fig. 16 : Boundary conditions of the test cell

Boundary condition # 1 : Due to the domain symmetry the axial mid plane of the Niobium specimen is a fictitious adiabatic wall. Excepting the heater location, all the external walls in the vacuum side of the specimen are also adiabatic.

Boundary condition # 2 : Heat flux is laterally introduced at the heater location. Notice that the problem must be formulated with axisymmetric boundary conditions (actual limitation of the POISNL code). The true resistor heater is replaced , for modelling purpose, by a lateral surface heating at the resistor location.

Boundary condition # 3 : The heat transfer at the Nioubium / Helium II interface is controlled by the Kapitza conductance $\mathbf{H_k}$.

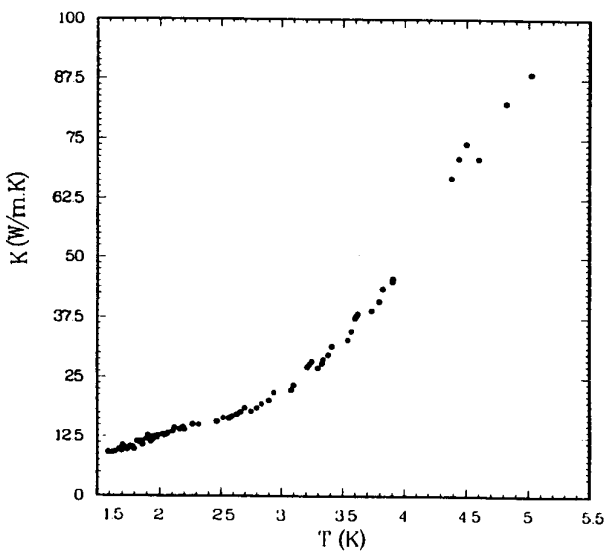

Fig. 17 : Thermal Conductivity of Niobium (Wah Chang 270)

Two important thermophysical input data are needed for precise calculations: the Niobium thermal conductivity **k(T)** and the Kapitza conductance $\mathbf{H_k(T)}$. The first parameter has been measured in situ by means of the A.B. resistors located on the heater post. The results (Fig. 17) were compared to those obtained with another experimental set up [Koechlin 1991] using test specimens machined from the same Niobium ingot : the two results are in agreement to within **±15%** .

The main source of error in **k(T)** measurements is due to the error in precisely locating the thermometers on the sample : a relative error of **10%** (i.e. 1 mm) on **Δz** leads to the same contribution to **k(T)** error. The AB resistors measure the mean temperature at three different points along the **z** direction, with **1.6** mm (AB resistor diameter) spread length at each point.

The second model parameter is the Kapitza conductance $\mathbf{H_k}$ which is unknown for our specimen. Fortunately,it is the only unknown parameter of the problem and its value can be adjusted by fitting the temperature distribution experimental data with numerical results. The radial temperature distribution **ΔT(r)**, measured by four AB resistors located on the Niobium plate (vacuum side) was used for this purpose. A trial and error method was adopted in order to estimate the Kapitza conductance. Starting from typical $\mathbf{H_k}$ values published by previous works [Mittag 1973] [Wilkes 1978] , the temperature field in the specimen was calculated and compared to the experimental results : **ΔT(r)** on the vacuum side and **ΔT(z)** along the heater post. This relatively straightforward method is very efficient and the convergence is obtained after less than 8 iterations. In order to accelerate the iteration process, the "vacuum" thermometer was used as a "guide" for $\mathbf{H_k}$ adjustment during the first steps : a coarse adjustement is obtained after 3 iterations. After that, the experimental radial temperature distribution on the heated side of the Niobium plate, is used for further refinement of the Kapitza conductance estimate. An example of $\mathbf{H_k}$ adjustment is shown in Fig. 18 displaying isotherms calculated by POISNL for **10 mW** input power and $\mathbf{T_{bath}}$ **= 1.6 K.** The isotherms in the heater post region where the axial gradient is measured are horizontal planes, giving high confidence in the **k(T)** experimental determination for the heater power range used during the tests **(P≤100 mW)**. In contrast , the isotherms inside the Niobium plate, are influenced by two important effects : a 2D effect due to the

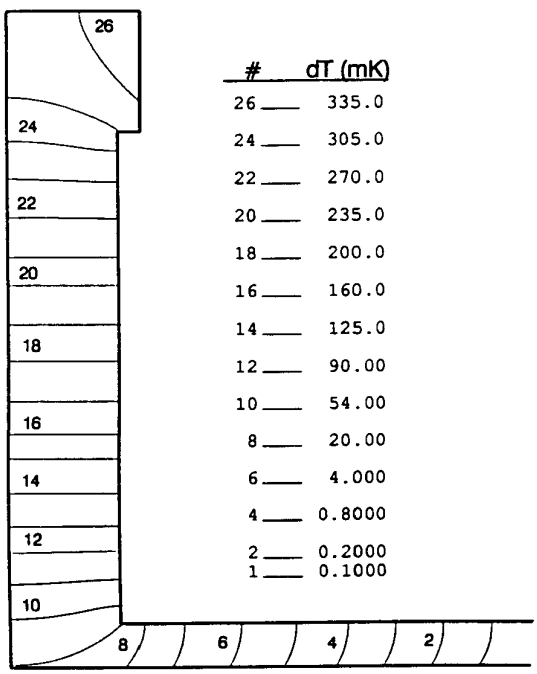

Fig. 18 : Isotherms calculated with POISNL code

radial diffusion and a temperature jump at the Niobium / Helium II interface. Concerning the radial temperature distribution (Fig. 19) , the experimental results are in good agreement with numerical data obtained with H_k = **0.19 W/cm².K** , T_{bath} = **1.6 K** and **P = 10 mW** .

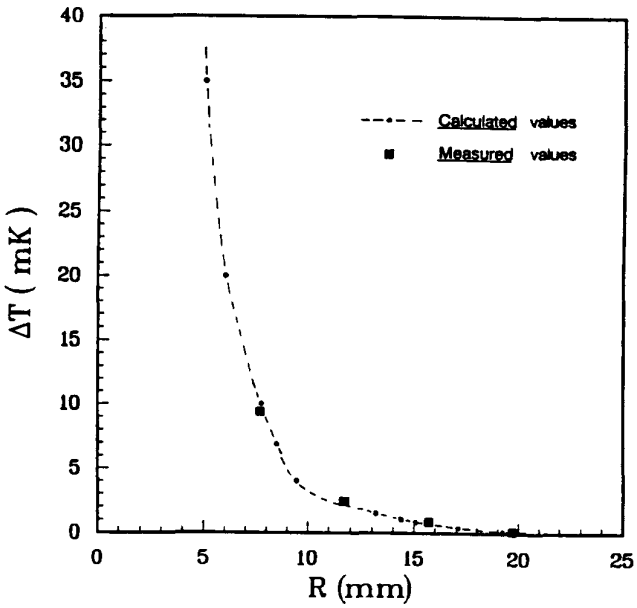

Fig. 19 : Radial temperature distribution of the test cell

The resulting thermometer efficiency is **88%** and the mean deviation from the calculated axial temperature distribution along the heater post was less than **10%** . These results were confirmed for a different heater power **(P=100mW)** , but in this case the H_k value was corrected using the measured bath temperature dependence ($\Delta T \propto T_{bath}^{-3.18}$) measured with vacuum thermometers in the TE011- like cell (see below) and the enhancement factor f_e for large heat power.

The results of two experimental studies on Niobium Kapitza conductance [Mittag 1973] [Wilkes 1978] are compared to our estimate in Table 1.

Table 1 : Kapitza Conductance Measurements of Niobium

Author	h_o	n	H_k @ 1.8 K
Mittag (1973)	0.017	3.62	0.143
" "	0.02	4.65	0.308
Wilkes (1978)	0.0136	3.99	0.142
" "	0.0252	3.90	0.249
" "	0.0072	4.41	0.096
" "	0.0145	3.96	0.149
" "	0.024	4.30	0.310
IPN-GECS (1991)	0.043	3.18	0.279

$H_k = h_o T_{bath}^n$ (W/cm² K)

As far as the absolute value of H_k at a given bath temperature, is compared to the previous works, a good agreement is obtained. In contrast, the $\hat{n}$ - exponent value vary in a large range ($3.6 < n < 4.6$) depending on the sample surface treatment, for the previous reported experiments. We have decided to use the value $n = 3.18$, which corresponds to the lower value obtained in an experiment reported in Section **3.4** . As discussed below, we have systematically found that high efficiency thermometers give a low bath temperature dependence , which is nearly constant within the heater power range. We consider at present, that these thermometers give an accurate measurement of the surface temperature and, consequently, of the real bath temperature dependence of ΔT at the Solid/Helium II interface.

3.4 TE011 - like calibration cell

Starting with the first vacuum thermometer prototypes, an array of 6 thermometers has been constructed and tested with the cell previously described section **2.2**, and following the same experimental procedure. Due to the radial size of this prototype (diameter of the vacuum flange), the number of thermometers was limited to a maximum of 6 , which are located on a circle corresponding to B_{max} ($r=26.4$ **mm**). The thermometers are connected to a common vacuum can using standard flanges (copper seals). Once this assembly has been pumped down to 10^{-3} - 10^{-4} **Torr** at room temperature, it was maintained under static vacuum by closing a special metal sealed valve, which is leak proof in superfluid Helium.

Calibration results: comparison with epoxy thermometers

The vacuum thermometer array was calibrated (ΔT **vs. P**) at different bath temperatures $1.52\ K \leq T_{bath} \leq 2.1\ K$. Some typical thermal response curves (Fig. 20) are compared to those obtained with epoxy thermometers using the same test assembly and Apiezon N grease as thermal bonding agent.

The results confirm a good linearity and a significant efficiency improvement by a factor α ($\alpha = \Delta T_{vacuum} / \Delta T_{epoxy}$, at given T_{bath} and heat power **P**). This enhancement factor has a strong dependence on T_{bath} , increasing from $\alpha \approx 2$ at $T_{bath} = 1.5\ K$, to $\alpha \approx 10$ at $T_{bath} = 2.1\ K$ (for $P = 100$ **mW**) .

The experimental data were compared to the model calculations described in section **2.2**, for $T_{bath} = 1.7\ K$ and $1.9\ K$, the results are summarized in Table **2** .

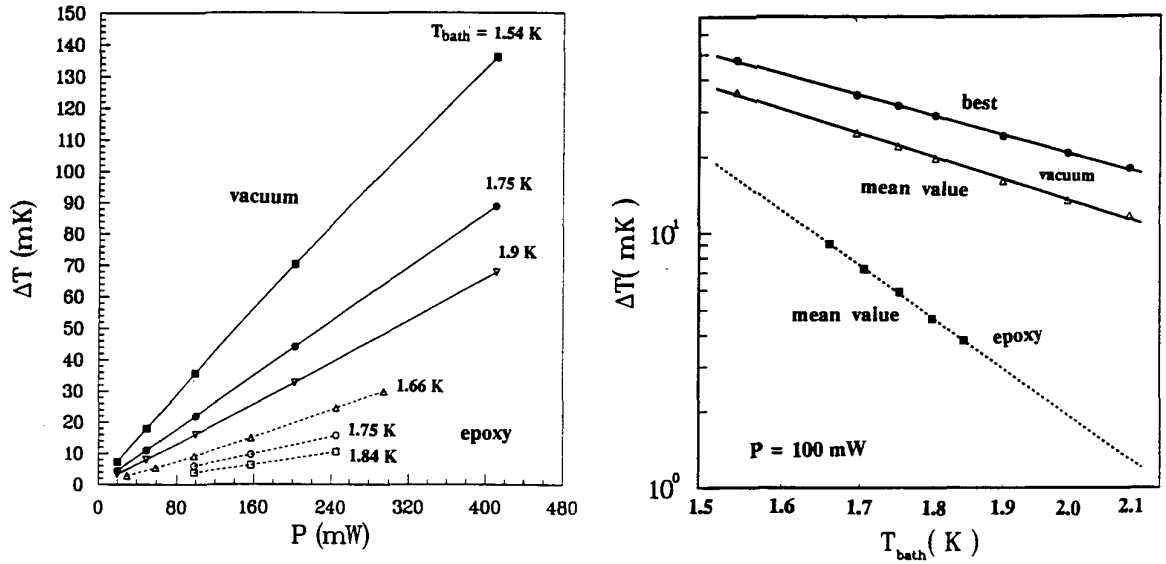

Fig. 20 : Comparison of epoxy and vacuum thermometers

Table 2 : Efficiencies of epoxy and vacuum thermometers

T_{bath}(K)	ΔT (mK) model	<ΔT> (mK) epoxy	<ΔT> (mK) vacuum	ΔT (mK) best	η (%) epoxy	η (%) vacuum
1.7	33.6	6.5	24.7	34.1	19	74
1.9	25.5	2.9	16.0	24.0	11	63

The T_{bath} dependence of the vacuum thermometers response has been extensively studied and the results are presented in Fig. 20 and Table 3 .

The experimental data fit well with a power law $\Delta T = A(P).\ T_{bath}^{-n}$, where the **A** parameter depends on the heater power **P** : the mean standard deviation of the fit was less than **3%** . The **n**- exponent ranges from **3.18** to **4.52** , which is in good agreement with the Kapitza conductance measurements reported by other authors. Furthermore, for all the sensors, this **n** - exponent has a weak heater power dependence ($\Delta n/n < 22\ \%$) , confirming the high efficiency of the vacuum thermal insulation which reduces possible effects of Helium II micro-channels inside the thermal bonding agent (Apiezon N grease) .

Notice than **n** is strongly correlated with the thermometer efficiency : a very efficient thermometer have **n** values close to **3** and a weak heater power dependence **(#2, #4 and #6)** . In that case the heat power dependence is not monotonic as it is the case for a less efficient thermometer **(#3)** , for which **n** decreases from **5.4** to **3.1** with

Table 3 : T_{bath} dependence of vacuum thermometers

Thermometer (#)	RMS(mK) @ P = 100 mW	< n >	σ_n(%)
1	0.07	4.03 ± 0.41	10
2	0.18	3.32 ± 0.11	3
3	0.46	4.52 ± 0.99	22
4	0.13	3.18 ± 0.11	3.6
5	0.08	3.51 ± 0.26	7.4
6	0.14	3.20 ± 0.16	3.7

RMS (mK) : Precision of the fit $\Delta T \propto T_{bath}^{-n}$, at P = 100 mW
< n > : Mean value of the n-exponent, over the heater power range (20 mW < P < 420 mW)
σ_n(%) : Mean relative standard deviation of n in the heater power range

increasing power. This behaviour is not clearly understood at the present, it may result from several effects : bad contact pressure and possibly Helium II channels inside the thermal bonding agent, or heat leaks at the wetted rim of the sensor tip.

Finally, one should note that even if these vacuum thermometers have an improved efficiency, as compared to epoxy thermometers, further development is needed in the future, in order to reduce the sensitivity dispersion which is probably due to the mounting system.

3.5 TE011 cavity measurements with vacuum thermometers

The experimental results presented in this section have been obtained with the TE011 vacuum thermometer array (6 thermometers) .

a) Surface temperature measurements on bulk Niobium end plates

Two samples (**Nb # 1 , Nb # 2**) made from Niobium sheets of **RRR = 180** have been studied. An example of temperature maps obtained with these samples is presented in Fig. 21 , for nearly the same magnetic induction level.

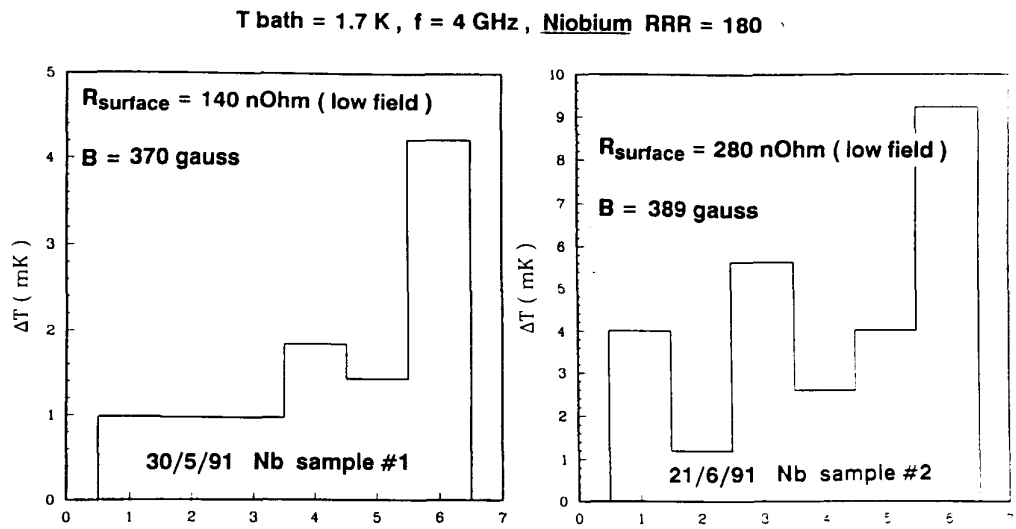

Fig. 21 : Temperature measurements on bulk Niobium samples

The more pronounced observed heating of **Nb # 2** sample can be attributed to its higher R_s value. However, one should point out the difficulty, for bulk Niobium end plates, of accurately estimating the contribution of the end plate R_s , to the total measured value which is proportional to the RF losses of the whole cavity.

The more interesting feature is the comparison (Fig. 22) of the **#6** thermometer response as a function of the magnetic induction, for the two samples. As explained before for the epoxy thermometers, a power law ($\Delta T \propto B^n$) was adopted to fit the experimental data leading to the following results:

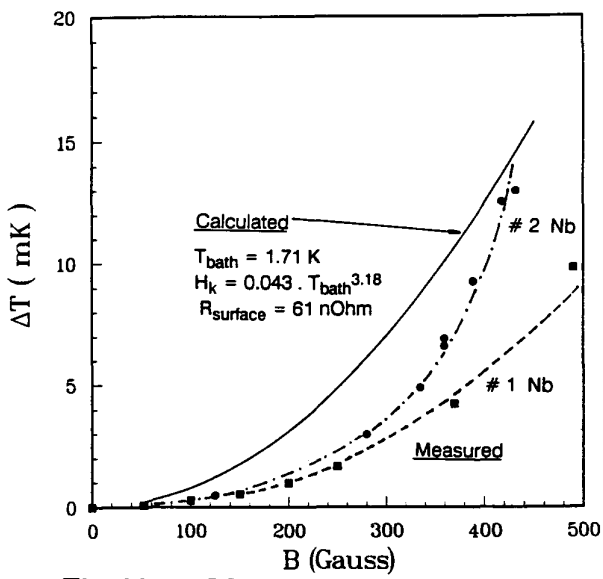

Fig. 22 : Magnetic field dependence of the thermal response

Nb # 1 $\Delta T \propto B^{2.1}$

Nb # 2 $\Delta T \propto B^{2.6}$

These experimental n-exponent values are consistent with those obtained with the epoxy thermometer array for small heating (i.e. $2 < n < 4$). As previously discussed, the departure from the quadratic dependence cannot be attributed neither to the epoxy thermometer efficiency, nor to its non linearity. In order to understand if this departure is due to a 2-D and a non

linear thermal effect inside the Niobium specimen, for "high" R_s values, an analytical solution of the heat equation has been used. In this model calculation R_s is taken to be uniform (defect free) over the whole surface, while the magnetic induction follows the distribution of the TE011 mode. The numerical results lead to the following fit, for two different values of R_s :

$$\Delta T \propto B^2 \quad \text{for} \quad R_s = 61 \text{ nOhms}$$

$$\Delta T \propto B^{2.02} \quad \text{for} \quad R_s = 150 \text{ nOhms}$$

Even at higher R_s ($R_s > 200$ nOhms) the fit of the model results gives a nearly quadratic behaviour, in the useful range of magnetic induction of this experiment. A significant increase of the exponent is obtained for magnetic field levels close to the quench region ($B_{max} > 1000$ gauss at 4 GHz). Calculations of thermal effects induced by small defects on the SC surface with enhanced losses (R_s(defect)≈8 mOhms), have also been performed leading to similar results as the defect free case. Hence, some aspects of the RF surface heating remains unexplained when described by a simple model : more elaborate RF losses description, getting more experimental data, and improving the thermal model calculations, may lead to a correct analysis of this phenomena.

b) NbTiN sputtered film

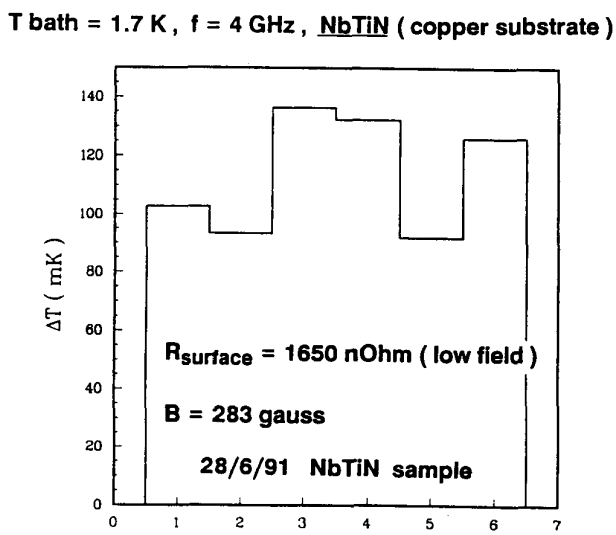

Fig. 23 : Temperature measurements on NbTiN sample

A sample of NbTiN sputtered on a copper substrate has been tested with the vacuum thermometer array (Fig. 23). Increased thermometer sensitivity allows an easy measurement of the surface heating. A low dispersion is observed between the 6 thermometers, but the number is too small to conclude on the homogeneity of R_s over the end plate surface. Notice that for this type of sample, the high value of the thermal conductivity of copper , compared to bulk Niobium samples, improves the radial heat diffusion in the plate.

Consequently , the temperature map observed on the Helium II cooled side, is not an homothetic picture of the temperature map at the vacuum side of the plate which is directly related to the RF losses.

Conclusions and future issues

Fixed epoxy thermometers are now intensively used to study thermal effects in a special TE011 cavity. An accurate calibration allow us to be confident on efficiency, reproducibility and linearity of these thermometers. We report the preliminary results with the TE011 cavity, showing interesting thermal effects which must be confirmed by systematic tests and model calculations.

The first vacuum thermometers prototypes, have been succesfully tested, leading to an improved sensitivity, by at least a factor of 2.5 in comparison with epoxy thermometers. The thermal response dependence on bath temperature is very close to the Kapitza resistance behaviour, according to both the theoretical predictions and the previous experimental results. Using a special calibration cell, a measurement of the Kapitza conductance has been performed which shows a good agreement with results reported by other authors.

Further developments of the vacuum thermometers are planned in the next future :

- size reduction together with a more reliable and simplified fabrication process.
- independent sealed static vacuum for each thermometer.

Concerning the calibration of these thermometers, two points are not completely understood by this time : the influence of the contact pressure, and the effect of heat leaks through the wetted rim of the sensor tip. More systematic studies of these factors and complementary model simulations are needed in order to provide a complete analysis of the vacuum thermometer response.

Acknowledgements

The authors would like to especially thank B. Aune, M. Juillard and A.Veyssière from the GECS group (C.E. Saclay) , M.X. François from the Laboratoire de Thermodynamique des Fluides (Univ. Paris VI), and R. Brizzi from the Centre de

Mathématiques Appliquées (Ecole Polytechnique, Palaiseau), for their continuous encouragement and competent advice.

Sincere thanks are given to the GECS group (C.E. Saclay and IPN Orsay), especially J. Gratadour, J.P. Charrier, N. Hammoudi, P. Dubois and M. Brient for their technical support during the experimental tests.

REFERENCES

Aune, B. , et al. Proceedings of the 14th Linear Accelerator Conference. Williamsburg (USA) . October 1988 CEBAF Report 89-001 , p. 432

Bernardou, M. , et al. " MODULEF : une bibliothèque modulaire d'éléments finis " INRIA (France) 2ème Edition . 1988

Brizzi, R. , et al. Proceedings of the ASME-Heat Transfer Conference Seattle (USA) . June 1990 ASME-HTD vol 134 , p. 15

Fouaidy, M. Ph. D. Thesis. Université Paris VI . January 1989

Fouaidy, M. IPNO Report 90-03. Orsay 1990

Gorter, G.J. and Mellink, J.H. Physica XV (1949) p. 285

Koechlin, F. and Dolégiéviez, P. " Measurements of Thermal Conductivity of Industrial Niobium " . This workshop.

Juillard, M. , et al. Proceed. European Particle Accelerator Conference (EPAC) Nice (France) June 1990 , p. 1106

Mittag, K. Cryogenics 13 (1973) p. 94

Müller, G. and Kneisel, P. Cornell University . LNS Report SRF-851201 (1985)

Padamsee, H. CERN/EF/RF Report 82-5 . July 1982

Padamsee, H. , et al. Particle Accelerator Conference Proceedings Washington DC . March 1987, p. 1824

Roberts, P.H. and Donnelly, R.J. Annual Review of Fluid Mechanics Vol. 6 (1974) p. 179

Tückmantel, J. CERN/EF/RF Report 84-6 . June 1984.

Wilkes, K.E. Ph. D. Thesis . Ohio State University (1978)